American Mineralogist, Volume 76, pages 1620–1627, 1991

Feldspars $MAlSi_3O_8$ (M = H, Li, Ag) synthesized by low-temperature ion exchange

JOACHIM DEUBENER,* MARTIN STERNITZKE, GERD MÜLLER
Institut für Mineralogie, Technische Hochschule Darmstadt, Schnittspahnstraße 9, D-6100 Darmstadt, Germany

ABSTRACT

Stable alkali feldspars $MAlSi_3O_8$ contain monovalent ions M ranging in radius from 1 Å to 1.5 Å. By low-temperature (~300 °C) ion exchange, feldspars of approximate composition $HAlSi_3O_8$, $LiAlSi_3O_8$, and $AgAlSi_3O_8$ have been synthesized. The exchange reactions can be reversed. However, only feldspars with essentially disordered Al-Si distributions yield the H form which is the precursor for the Li and Ag forms. Lithium and silver feldspars are triclinic and similar to analbite. They both obey the trends established for natural alkali feldspars that describe the influence of ionic size on structure, lattice parameters, and thermal transformations. Hydrogen feldspar, because of the completely different coordination requirements of H compared to other monovalent ions, differs significantly from the alkali feldspars.

INTRODUCTION

Stable alkali feldspars $MAlSi_3O_8$ are known for ions ranging in size from 1 Å (Na) to 1.5 Å (Rb). Feldspars of approximate composition $HAlSi_3O_8$ and $LiAlSi_3O_8$ have been prepared from a natural sanidine by low-temperature (~300 °C) ion exchange (Müller, 1988). $LiAlSi_3O_8$ is triclinic with lattice parameters fitting an extension of the $KAlSi_3O_8$-$NaAlSi_3O_8$ series quite well. $HAlSi_3O_8$ is monoclinic and does not fit into the alkali feldspar series. The framework structure of $HAlSi_3O_8$ as derived from single-crystal X-ray data has been reported (Paulus and Müller, 1988), but the protons have not been located; they probably are highly disordered, as evidenced also by neutron powder diffraction.

The ion exchange processes can be reversed. This implies that the framework topology and Al-Si order are not affected.

In this paper, we report on further experiments to introduce H, Li, Cu, and Ag ions into feldspar frameworks of different degrees of Al-Si order and on the properties of the feldspars that have been synthesized.

MATERIALS AND EXPERIMENTAL METHODS

Natural alkali feldspars were used as starting materials; their composition, lattice parameters, and degree of Al-Si order as derived from lattice constants (Kroll and Ribbe, 1983) are listed in Table 1. These feldspars cover the range of Al-Si order from high sanidine (I) to low microcline (VII), the two microcline types being perthitic. Most experiments were made with the sanidine from Volkesfeld, Eifel (II), a low-sanidine sample that has been studied in much detail before (e.g., Bertelmann et al., 1985; Beran, 1986). The other samples were taken from the Tamnau collection of the authors' institute.

Details of the ion exchange processes have been described elsewhere (Müller et al., 1988; Müller, 1988). Schematically the sequence of exchange steps is

$$\text{NaCl} \quad \begin{matrix} KAlSi_3O_8 \\ \downarrow \\ NaAlSi_3O_8 \end{matrix} \quad 3\text{ d, }820\text{ °C} \qquad (1)$$

* Present address: Institut für Nichtmetallische Werkstoffe der Technischen Universität Berlin, Englische Straße 20, D-1000 Berlin 12, Germany.

TABLE 1. Natural alkali feldspars used for ion exchange experiments

No.	Type	Loading	Composition (mol%)*				Lattice constants
			Ab	Or	An	Ce	a (Å)
I	Sanidine	Drachenfels, Germany	39.1	55.1	4.9	0.9	8.435(6)
II	Sanidine**	Volkesfeld, Eifel, Germany	16.0	82.2	0.7	1.1	8.544(4)
III	Orthoclase	Elba, Italy	21.8	74.3	3.5	0.4	8.526(5)
IV	Orthoclase	Loket near Karlsbad, CSR	21.7	74.4	3.3	0.6	8.566(7)
V	Adularia	St. Gotthard, Switzerland	14.4	84.6	0.8	0.2	8.570(3)
VI	Microcline†	Pechbrunn, Bavaria, Germany	24.3	73.3	1.8	0.6	8.578(9)
VII	Microcline†	Arendal, Norway	22.1	76.2	1.6	0.1	8.571(4)

* Calculated from atomic absorption analysis.
** Sanidine of this locality is somewhat variable in composition; Müller (1988) used a different sample.
† Both microcline samples are perthitic, composition is overall, lattice constants are for potassium feldspar phase only.

0003–004X/91/0910–1620$02.00

$$H_2SO_4 \quad \downarrow \quad 4\text{ d, }320\text{ °C} \qquad (2)$$
$$HAlSi_3O_8$$

$$MNO_3 \quad \downarrow \quad 280\text{–}300\text{ °C.} \qquad (3)$$
$$MAlSi_3O_8$$

The first, high-temperature exchange to a sodium feldspar is necessary because potassium feldspars, even as fine powders, do not react directly with H_2SO_4, probably because K mobilities are too low. In hot, concentrated H_2SO_4, the Na ions can be exchanged with protons at temperatures around 300 °C. Finally, in Step 3 the protons are exchanged with univalent ions. Molten nitrates were used as sources of Li and Ag ions. In the case of $AgNO_3$, the reaction mixture was sealed into pyrex glass tubes to prevent decomposition of the nitrate. Various low-melting salt mixtures (e.g., CuCl-CuI) were tried unsuccessfully as sources for Cu ion exchange (see below). All ion exchange products could be reexchanged in molten $NaNO_3$ at 300 °C to a sodium feldspar with lattice constants identical to those after Step 1.

Results of ion exchange experiments

The first series of exchange experiments was conducted with sanidine from Volkesfeld, Eifel, Germany (II, Table 1). The H and Li forms could be obtained readily; they have been described by Müller (1988). After reaction of the H form with molten $AgNO_3$ at 275 °C for 5 d, partial Ag-H exchange had occurred; after four repetitive experiments the product was essentially pure $AgAlSi_3O_8$. Lattice constants and composition of this and the other exchange products are given in Table 2. $AgAlSi_3O_8$ is triclinic, space group $C\bar{1}$; its lattice constants are similar to those of analbite but with α and γ deviating less from 90°.

All attempts to substitute Cu^+ ions for H^+ or Li^+ were unsuccessful. From ionic radii, Cu^+ should be intermediate between Na^+ and Li^+. It appears that molten salts that contain monovalent Cu are so strongly complexed that they do not contain enough free Cu^+ ions for exchange.

A comparison of the X-ray diffraction patterns of the various phases made from Volkesfeld sanidine is shown in Figure 1. It is evident that they are all feldspar-type phases but with considerable differences in lattice constants.

The same sequence of exchange reactions was attempted with the other feldspars from Table 1. Results are also compiled in Table 2. Surprisingly, only feldspars I–V, i.e., the ones with topochemically monoclinic Al-Si distributions, gave the H phase upon reaction with H_2SO_4. The Na equivalent of the intermediate microcline, VI, did lose much of its Na content but at the same time became gradually amorphous, whereas sample VII didn't react at all. From the H forms of samples I–V, only III and V were further treated to yield the Li and Ag forms.

Thermal properties of ion exchanged samples II

Powder X-ray diffraction at elevated temperatures was investigated with a Guinier–De Wolff camera equipped with a sample heating system (Enraf-Nonius). The thermal instability of hydrogen feldspar has been reported before (Müller, 1988): upon heating in air it gradually gives off an amount of H_2O equivalent to its H content and simultaneously becomes amorphous. The lithium feldspar is stable up to about 900 °C; at higher temperatures it decomposes into a mixture of β-quartz-type and keatite-(β-spodumene-) type lithium aluminosilicates. Silver feldspars can be heated at least to 800 °C; higher temperatures have not been studied. Table 3 contains axial and volume expansion coefficients. The principal axes of the thermal ellipsoids and their orientations are given in Table 4.

Cell angles α and γ become less oblique on heating in both lithium and silver feldspars. The silver feldspar, in a pattern similar to analbite, transforms reversibly into a monoclinic phase, space group $C2/m$, at 550 ± 20 °C. This inversion temperature is probably influenced by the partial Al-Si order of the particular sanidine used here as well as by the residual K and Ba contents. The Na-rich equivalent transformed to monalbite at 820 ± 20 °C instead of ~950 °C for pure, fully disordered analbite, in qualitative agreement with the correlations of Kroll (1984). In lithium-feldspar, extrapolation of the splitting of the $(1\bar{1}\bar{1})/(11\bar{1})$ and $(130)/(1\bar{3}0)$ diffraction peaks to zero indicates a very high transformation temperature of about 1600–1900 °C.

Table 1—*Continued*

Lattice constants							
b (Å)	c (Å)	α (°)	β (°)	γ (°)	$t_1(o)$	$1_1(m)$	$t_2(o) = t_2(m)$
13.010(3)	7.171(2)	90	116.17(4)	90	0.29(5)		
13.010(3)	7.194(4)	90	115.99(4)	90	0.32(5)		
13.020(3)	7.188(2)	90	116.07(4)	90	0.32(5)		
12.985(4)	7.201(2)	90	115.98(5)	90	0.40(5)		
12.975(3)	7.212(2)	90	115.98(2)	90	0.44(5)		
12.969(8)	7.210(4)	90.99(23)	115.96(8)	88.28(15)	0.81(5)	0.09(5)	0.05(5)
12.956(3)	7.216(1)	90.62(4)	115.94(3)	87.65(4)	0.99(5)	0.02(5)	0.00(5)

Table 2. Composition and lattice constants of ion exchanged feldspars

		Composition (mol% M)						Lattice constants					
		Li	Na	Ag	K	Ca	Ba	*a* (Å)	*b* (Å)	*c* (Å)	α (°)	β (°)	γ (°)
Sodium feldspars	I*	—	83.6	—	11.6	4.3	0.5	8.172(9)	12.884(6)	7.121(3)	93.23(8)	116.49(6)	90.33(9)
	II	—	91.6	—	7.0	0.7	0.7	8.167(8)	12.856(9)	7.120(4)	93.34(6)	116.40(6)	90.22(8)
	III	—	92.9	—	2.5	4.5	0.1	8.162(6)	12.864(4)	7.118(2)	93.36(5)	116.53(4)	90.27(7)
	IV	—	89.3	—	6.3	3.6	0.8	8.173(7)	12.849(6)	7.150(2)	93.20(8)	116.52(5)	89.92(10)
	V	—	93.2	—	5.6	0.8	0.4	8.164(6)	12.828(4)	7.157(2)	93.01(5)	116.60(5)	90.18(7)
	VI	—	94.3	—	4.5	1.2	0.0	8.155(4)	12.824(8)	7.156(3)	93.54(8)	116.77(5)	88.26(10)
	VII	—	94.1	—	4.6	1.3	0.0	8.145(5)	12.798(6)	7.160(3)	93.99(11)	116.56(8)	87.76(5)
Hydrogen feldspars	I	—	9.3	—	7.2	3.5	0.9	7.946(8)	13.152(6)	7.190(3)	90	116.26(8)	90
	II	—	7.2	—	2.7	0.3	0.8	7.946(5)	13.131(7)	7.189(4)	90	116.57(6)	90
	III	—	3.1	—	1.8	2.0	0.2	7.922(7)	13.149(5)	7.204(3)	90	116.35(7)	90
	IV	—	10.4	—	3.8	1.9	0.8	7.964(9)	13.126(7)	7.226(4)	90	116.58(10)	90
	V	—	3.3	—	4.3	0.2	0.3	7.950(6)	13.097(4)	7.249(2)	90	116.86(6)	90
Lithium feldspars	II	89.5	5.2	—	2.5	0.2	0.8	7.878(2)	12.690(5)	7.046(3)	95.89(4)	116.78(3)	90.13(3)
	III	91.3	3.0	—	1.9	2.1	0.2	7.860(3)	12.681(3)	7.051(1)	96.09(3)	116.82(2)	89.95(2)
	V	90.7	3.1	—	4.0	0.2	0.3	7.850(6)	12.631(5)	7.071(3)	96.24(7)	116.83(5)	89.92(6)
Silver feldspars	II	—	7.4	84.0	2.9	0.3	0.7	8.221(6)	12.968(5)	7.160(3)	91.83(5)	116.80(6)	90.10(5)
	III	—	3.3	88.0	2.1	2.1	0.2	8.229(5)	12.951(4)	7.156(2)	92.73(4)	116.86(5)	90.17(5)
	V	—	3.5	87.1	4.5	0.2	0.2	8.227(8)	12.913(6)	7.190(3)	92.34(6)	116.74(7)	90.10(7)

* See Table 1 for symbols I–V.

Interpretation of the experimental data and the modeling of the structures

The results described above show that only alkali feldspars with rather disordered Al-Si distributions can be ion exchanged to hydrogen feldspars. These hydrogen feldspars apparently also have very disordered proton distributions, as has been stated in the introduction. Electrostatic charge balance considerations suggest that the protons should be bonded preferentially to those O atoms bonded to Al atoms. In this case, the proton disorder would reflect the Al-Si disorder. Consequently, in feldspars with ordered Al-Si distributions the proton distributions would also be ordered. For other hydrogen aluminosilicates it has been shown that ordered proton distributions can cause considerable framework strain resulting from H bond formation (Effenberger and Müller, 1988; Vogt et al., 1990). Conceivably, the feldspar framework cannot tolerate such strain, but further work is needed to clarify this problem.

For natural alkali feldspars, plots of the lattice constants *b* vs. *c* or α^* vs. γ^* are convenient to evaluate structural state and composition (Wright and Stewart, 1968; Smith and Brown, 1988). The general trends in the *b*/*c* plot are followed quite well by the synthetic lithium and silver feldspars; see Figure 2. For a given degree of Al-Si order they plot on the same straight lines as their Na and K equivalents, with Ag between Na and K and Li beyond Na as should be expected from ionic radii. This shows that, as far as the lattice constants *b* and *c* are concerned, the pattern of framework deformation created by variations of the monovalent cations remains the same over a remarkably wide range. The same is true for the *a* axis as can be seen from Table 2 and will be further discussed below.

The hydrogen feldspars do not fit into the general trends. This is because protons, unlike other cations, do not form an MO_x polyhedron that either bolsters or contracts the framework cavity about the M position. In particular, the very long *b* axis is a consequence of this (Paulus and Müller, 1988).

In the α^* vs. γ^* diagram, Figure 3, all monoclinic feldspars plot together. The triclinic silver feldspar equivalents of II, III, and V are located on the sanidine-analbite line, the lithium feldspars again on an extension beyond the analbite point. The feldspars with the same kind of cation do not coincide, probably because they contain residual contents different from other cations.

If the special case of the hydrogen feldspars is disregarded, lattice constants vary regularly with cation size in the whole $MAlSi_3O_8$ series. This is essentially also true

Table 3. Thermal expansion coefficients of H, Li, and Ag forms of Volkesfeld sanidine

	Space group	*T* (°C)	α (10^{-6} K^{-1})			
			α_a	α_b	α_c	α_V
$HAlSi_3O_8$	*C*2/*m*	25–400	25(4)	−2(2)	−3(3)	22(6)
$LiAlSi_3O_8$	*C*$\bar{1}$	25–800	17(2)	13(1)	11(2)	43(3)
$AgAlSi_3O_8$	*C*$\bar{1}$	25–550	18(3)	2(1)	1(1)	25(4)
	*C*2/*m*	550–760	6(7)	6(4)	4(3)	17(12)

Table 4. Principal axes of thermal expansion ellipsoids and their orientations

	$HAlSi_3O_8$	$LiAlSi_3O_8$	$AgAlSi_3O_8$	
T (°C)	25–400	25–800	25–550	550–760
α_1 (10^{-6} K^{-1})	−4(3)	−1(2)	−31(4)	4(6)
a (°)	104(5)	100(4)	98(3)	129(49)
b (°)	90	136(2)	136(1)	90
c (°)	12(11)	41(2)	47(1)	13(52)
α_2 (10^{-6} K^{-1})	−2(2)	27(3)	38(4)	6(4)
a (°)	90	94(5)	79(16)	90
b (°)	0	46(2)	49(2)	0
c (°)	90	53(3)	57(3)	90
α_3 (10^{-6} K^{-1})	27(4)	15(2)	18(2)	7(13)
a (°)	14(1)	10(7)	13(2)	39(46)
b (°)	90	94(4)	103(6)	90
c (°)	102(5)	107(4)	119(3)	77(60)

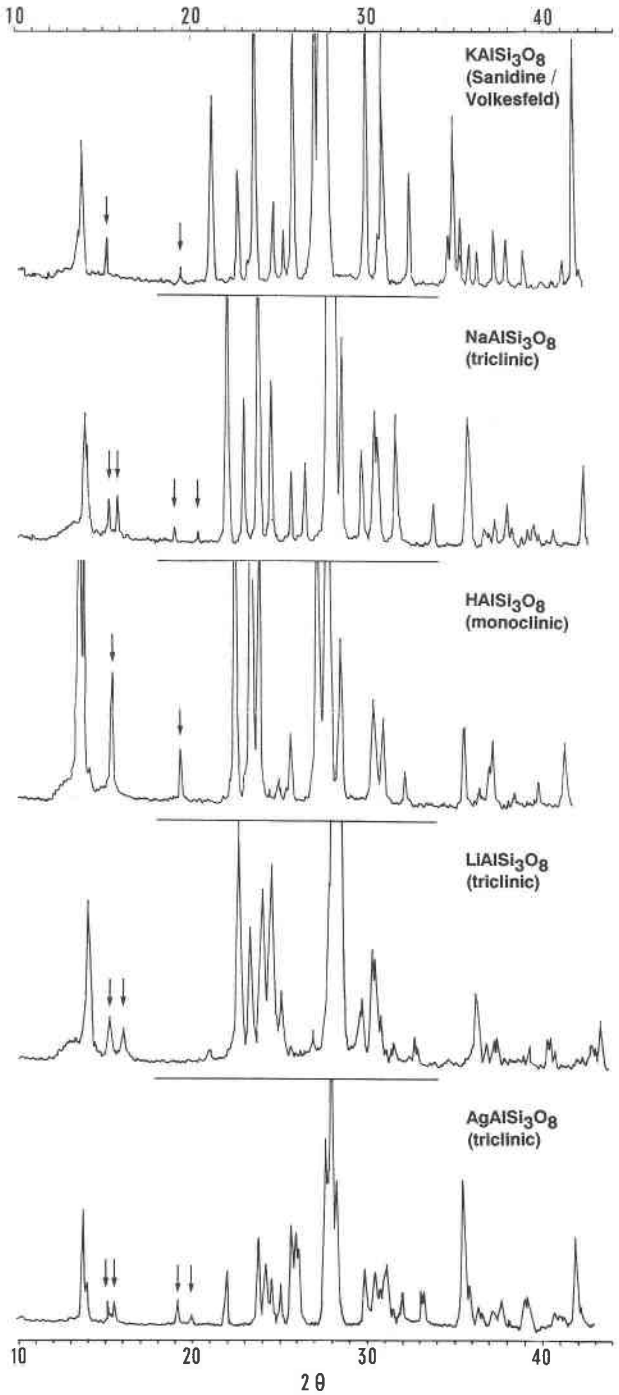

Fig. 1. X-ray powder diffraction patterns (Cu$K\alpha$) of sanidine from Volkesfeld, Eifel, and its Na, H, Li, and Ag equivalents. Peak splitting in triclinic feldspars marked by arrows.

for thermal properties. Figure 4 shows how the $C\bar{1}$ to $C2/m$ transformation temperature depends on ionic size: from lithium to silver feldspars it decreases continuously. The data of Kroll (1984) for the sanidine-analbite series fit the curve very well if average ionic radii for the (Na,K)-solid solution feldspars are used.

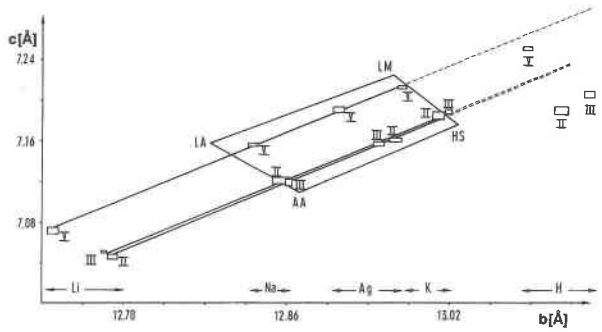

Fig. 2. Plot of b vs. c parameters from natural end-members and ion exchanged alkali feldspars. LA = low albite, AA = analbite, LM = low microcline, HS = high sanidine. See Table 1 for symbols I–V.

Thermal expansion in the alkali feldspars increases with decreasing size of the cations (Henderson, 1979; Kroll, 1984). As Table 3 shows, lithium feldspars, having a very large volume thermal expansion, and silver feldspars in the triclinic state follow this trend. Axial expansion is largest for the a axis in all feldspars $MAlSi_3O_8$. In sanidine and hydrogen feldspar, axial expansions in the b and c directions are quite small or even negative. For feldspars with small cations, b and c expansion becomes more important; in lithium feldspars all axial expansions are comparable.

In the monoclinic high-temperature state, the thermal expansion of silver feldspar is considerably smaller than in the triclinic state. Henderson (1979) measured the thermal expansion of an analbite containing 19 mol% $KAlSi_3O_8$ that had lattice constants and a transformation temperature very similar to the silver feldspars investigated here. It is surprising that for this analbite the thermal expansion increased above the transformation temperature. Additional measurements would be needed to confirm this apparent discrepancy.

The data discussed above strongly suggest that no major or unexpected structural changes occur in feldspars

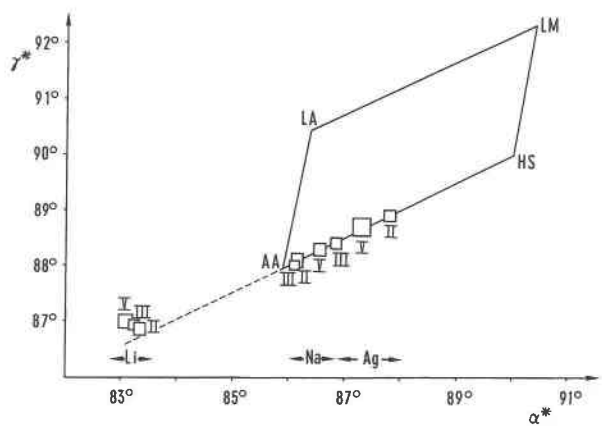

Fig. 3. Plot of α^* vs. γ^* parameters from natural end-members and ion exchanged alkali feldspars. See Figure 2 for symbols.

TABLE 5. Atomic coordinates of disordered feldspars $MAlSi_3O_8$ from DLS modeling and structure determinations

	$HAlSi_3O_8$ (DLS)			$LiAlSi_3O_8$ (DLS)			$NaAlSi_3O_8$ (DLS)		
	x/a	*y/b*	*z/c*	*x/a*	*y/b*	*z/c*	*x/a*	*y/b*	*z/c*
M	n.b.	n.b.	n.b.	0.2259	0.0046	0.0965	0.2576	0.0097	0.1089
$T_1(o)$	0.0256	0.1789	0.2231	0.0182	0.1470	0.2194	0.0109	0.1639	0.2323
$T_1(m)$				0.0183	0.8177	0.2333	0.0104	0.8207	0.2312
$T_2(o)$	0.6883	0.1185	0.3436	0.6696	0.0983	0.3037	0.6821	0.1056	0.3300
$T_2(m)$				0.6760	0.8789	0.3597	0.6922	0.8850	0.3577
$O_A(1)$	0.0	0.1321	0.0	0.0004	0.1284	0.9771	0.0028	0.1524	0.9975
$O_A(2)$	0.6144	0.0	0.2995	0.5577	0.0184	0.2542	0.5791	0.9899	0.2615
$O_B(o)$	0.8578	0.1347	0.2748	0.8282	0.0892	0.2136	0.8149	0.1206	0.2148
$O_B(m)$				0.8359	0.8516	0.2751	0.8230	0.8591	0.2415
$O_C(o)$	0.0138	0.3038	0.2091	0.0296	0.2744	0.2968	0.0481	0.2872	0.3176
$O_C(m)$				0.0186	0.6882	0.1889	0.0263	0.6947	0.2578
$O_D(o)$	0.2313	0.1441	0.4075	0.2124	0.0926	0.3788	0.1775	0.0933	0.3889
$O_D(m)$				0.2190	0.8648	0.4373	0.1919	0.8832	0.4143

	$AgAlSi_3O_8$ (DLS)			$KAlSi_3O_8$ (DLS)			$RbAlSi_3O_8$ (DLS)		
	x/a	*y/b*	*z/c*	*x/a*	*y/b*	*z/c*	*x/a*	*y/b*	*z/c*
M	0.2567	0.0045	0.1144	0.2814	0.0	0.1266	0.2881	0.0	0.1389
$T_1(o)$	0.0057	0.1712	0.2296	0.0074	0.1846	0.2302	0.0092	0.1891	0.2299
$T_1(m)$	0.0058	0.8201	0.2292						
$T_2(o)$	0.6863	0.1094	0.3346	0.7087	0.1156	0.3494	0.7198	0.1176	0.3454
$T_2(m)$	0.6925	0.8855	0.3508						
$O_A(1)$	0.0013	0.1575	0.9986	0.0	0.1680	0.0	0.0	0.1672	0.0
$O_A(2)$	0.5885	0.9946	0.2658	0.6308	0.0	0.2715	0.6571	0.0	0.2671
$O_B(o)$	0.8095	0.1304	0.2114	0.8193	0.1516	0.2229	0.8257	0.1614	0.2235
$O_B(m)$	0.8145	0.8586	0.2268						
$O_C(o)$	0.0402	0.2935	0.3059	0.0443	0.3061	0.2978	0.0531	0.3105	0.2917
$O_C(m)$	0.0264	0.6961	0.2714						
$O_D(o)$	0.1719	0.1023	0.3969	0.1638	0.1140	0.4009	0.1577	0.1174	0.4034
$O_D(m)$	0.1810	0.8842	0.4118						

	$NaAlSi_3O_8$*			$KalSi_3O_8$**			$RbAlSi_3O_8$†		
	x/a	*y/b*	*z/c*	*x/a*	*y/b*	*z/c*	*x/a*	*y/b*	*z/c*
M	0.2737	0.0073	0.1329	0.2846		0.1378	0.2958	0.0	0.1468
$T_1(o)$	0.0090	0.1650	0.2148	0.0094	0.0	0.2238	0.0104	0.1904	0.2227
$T_1(m)$	0.0048	0.8145	0.2290		0.1844				
$T_2(o)$	0.6902	0.1079	0.3202	0.7077	0.1177	0.3443	0.7227	0.1195	0.3440
$T_2(m)$	0.6849	0.8776	0.3535						
$O_A(1)$	0.0055	0.1351	0.9835	0.0	0.1462	0.0	0.0	0.1525	0.0
$O_A(2)$	0.5916	0.9907	0.2783	0.6343	0.0	0.2857	0.664	0.0	0.283
$O_B(o)$	0.8212	0.1084	0.1990	0.8276	0.1454	0.2266	0.832	0.1596	0.226
$O_B(m)$	0.8184	0.8470	0.2455						
$O_C(o)$	0.0162	0.2902	0.2770	0.0331	0.3100	0.2537	0.0464	0.3145	0.263
$O_C(m)$	0.0213	0.6873	0.2180						
$O_D(o)$	0.1959	0.1123	0.3876	0.1813	0.1265	0.4048	0.1682	0.1283	0.403
$O_D(m)$	0.1885	0.8675	0.4266						

* Prewitt et al. (1976).
** Gering (1985).
† Gasperin (1971).

upon substitution of Na or K ions by Li or Ag ions. No structural data are available for lithium or silver feldspars. A Rietveld refinement of lithium feldspar (from sample V) has been tried but did not yield conclusive results because of a very unfavorable ratio of free parameters to well-resolved diffraction peaks.

Modeling of the structures with the distance-least-squares (DLS) program originally developed by Meier and Villiger (1969) and modified by Baerlocher et al. (1978) was therefore attempted. With weight factors of 2.0 for T-O distances, 1.0 for O-O distances, and 0.2 for M-O distances this program gave good results for related aluminosilicate structures (Sternitzke and Müller, 1991). The same factors were used here. The consistency of the results was checked against those from structure determinations for rubidium, potassium, and sodium feldspars. Identical framework topology and disordered Al-Si distribution were assumed for all calculations. The main problem then is the MO_x coordination polyhedron. In a first series of calculations, the lattice constants were treated as free parameters, and the number of O atoms assumed to participate in M-O bonding was varied. Surprisingly, even rather distant O atoms had to be considered as bonding to achieve a satisfactory match of lattice constants. The model giving closest agreement was then used for further refinements with fixed, measured cell parameters. Final atomic parameters are listed in Table 5, with parameters for disordered sodium, potassium, and rubid-

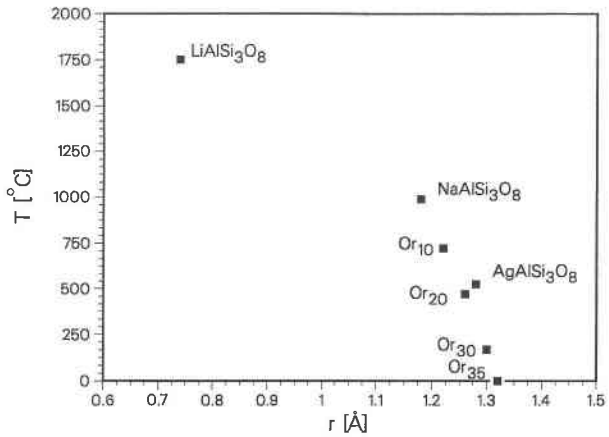

Fig. 4. Temperature of the triclinic/monoclinic transformation in disordered feldspars $MAlSi_3O_8$ as a function of cation radius (for observed coordination). Data for sanidine-analbite series from Kroll (1984).

ium feldspars from structure determinations also given for comparison. Average deviations between both sets of data are about 0.01, which is considered satisfactory because the feldspars used for the structure determinations were neither pure end-members nor fully disordered. Table 6 contains M-O distances and their electrostatic bond valence contributions (Brown and Altermatt, 1985). Again, the agreement between DLS-derived and diffraction-derived structures is acceptable. It is concluded that the model structures for $LiAlSi_3O_8$ and $AgAlSi_3O_8$ are also reasonably close to the actual structures of these phases. If all O atoms contributing at least 0.03 electrostatic valence units are considered part of the MO_x polyhedron, then the following coordination numbers result: Rb: X (+ I), K: X (+ I), Ag: VIII (+ III), Na: VIII (+ III), and Li: V (+ III). The numbers in parentheses are the additional O atoms that contribute very little (<0.01) to bonding but were nevertheless essential for the DLS refinements.

The coordination of Ag is quite similar to that of Na: five O atoms are close and three are farther away. In the series from K through Ag to Na, the preference for the five O atoms $O_A(1)$, $O_A(1)$, $O_A(2)$, $O_B(o)$, and $O_D(o)$ is clearly developed. They approach ever more closely at the expense of the others. In lithium feldspar this trend appears to reach its extreme: the same five O atoms are attracted to distances between 2.2 and 2.4 Å, whereas all others are pushed out into nonbonding distances. Figure 5 shows the O atom environments of the cations in disordered potassium, sodium, and lithium feldspars in a projection onto (010). Ionic radii are drawn to scale for the coordination numbers given above (Shannon, 1976). Positions are taken from the DLS refinements; deviations from the structure analysis results are roughly twice the line thickness in Figure 5. All O atoms that are not considered as bonded are marked with an asterisk.

It can be seen from Figure 5 how the preference for O

Table 6. M-O distances and bond valences (in parentheses) in feldspars $MAlSi_3O_8$ from DLS modeling and structure determinations

	$LiAlSi_3O_8$	$NaAlSi_3O_8$	$AgAlSi_3O_8$	$KAlSi_3O_8$	$RbAlSi_3O_8$
$O_A(1)$	2.295(0.11)	2.656(0.10)	2.715(0.09)	3.077(0.08)	3.189(0.08)
$O_A(1)$	2.296(0.11)	2.791(0.07)	2.846(0.07)		
$O_A(2)$	2.368(0.09)	2.375(0.21)	2.446(0.20)	2.697(0.22)	2.971(0.15)
$O_A(2)$	3.595(0.00)	3.444(0.01)	3.484(0.01)	3.259(0.05)	3.161(0.09)
$O_A(2)$	4.083(0.00)	4.041(0.00)	4.029(0.00)	4.052(0.01)	4.075(0.01)
$O_B(o)$	2.234(0.13)	2.607(0.11)	2.748(0.09)	3.007(0.09)	3.145(0.09)
$O_B(m)$	3.203(0.01)	2.923(0.05)	2.877(0.06)		
$O_C(o)$	3.753(0.00)	3.665(0.01)	3.532(0.01)	3.240(0.05)	3.243(0.07)
$O_C(m)$	3.079(0.01)	3.032(0.04)	3.105(0.03)		
$O_D(o)$	2.225(0.13)	2.544(0.13)	2.676(0.10)	2.971(0.10)	3.036(0.12)
$O_D(m)$	3.148(0.01)	3.017(0.04)	2.990(0.05)		
ΣS	(0.59)	(0.77)	(0.71)	(0.92)	(0.99)
		$NaAlSi_3O_8$*		$KAlSi_3O_8$**	$RbAlSi_3O_8$†
$O_A(1)$		2.606(0.11)		2.899(0.13)	3.068(0.13)
$O_A(1)$		2.704(0.09)			
$O_A(2)$		2.340(0.23)		2.697(0.22)	2.949(0.16)
$O_A(2)$		3.552(0.01)		3.403(0.03)	3.250(0.07)
$O_A(2)$		3.822(0.00)		3.888(0.01)	3.939(0.01)
$O_B(o)$		2.512(0.15)		3.026(0.09)	3.168(0.09)
$O_B(m)$		3.186(0.03)			
$O_C(o)$		3.371(0.01)		3.125(0.07)	3.124(0.10)
$O_C(m)$		2.917(0.05)			
$O_D(o)$		2.497(0.15)		2.942(0.11)	3.039(0.12)
$O_D(m)$		3.133(0.03)			
ΣS		(0.86)		(1.06)	(1.12)

* Prewitt et al. (1976).
** Gering (1985) (sample SAGA without heat treatment).
† Gasperin (1971).

atoms $O_B(o)$ and $O_D(o)$ in sodium and particularly lithium feldspar causes ever larger deviations from monoclinic symmetry. The largest dimensional change of the polyhedron occurs approximately in [$\bar{2}$01] direction, which is given in Figure 5 by the vector connecting the $O_A(2)$ atom with the center between the two $O_A(1)$ atoms. The length of this vector decreases from 4.9 Å in potassium feldspar through 4.3 Å for sodium feldspar to 3.9 Å for lithium feldspar, i.e., by the amount of the ionic radius differences. These variations also affect the *a*-axis; the concomitant changes are only slightly smaller (8.54 Å → 8.15 Å → 7.88 Å).

Cell dimensions and structural modeling indicate that the small Li ions exert considerable strain on the feldspar framework. Yet, proper charge balance for the Li ions is not attained. The balance is not even attained for the Na ions, as can be seen from the bond valence sums in Table 6. A balance apparently is established between framework wrinkling and M-O bond lengths. T-O-T angles of the framework should be sensitive indicators. However, they cannot be derived from DLS refinements with sufficient accuracy, mainly because the TO_4 tetrahedra tend to be more regular than those from structure determinations. The increased kinking of the bands of four rings in *a* direction with smaller cation size, however, can be clearly seen in a projection of the tetrahedral nodes of the framework of potassium, sodium, and lithium feldspars onto (010) (see Fig. 6).

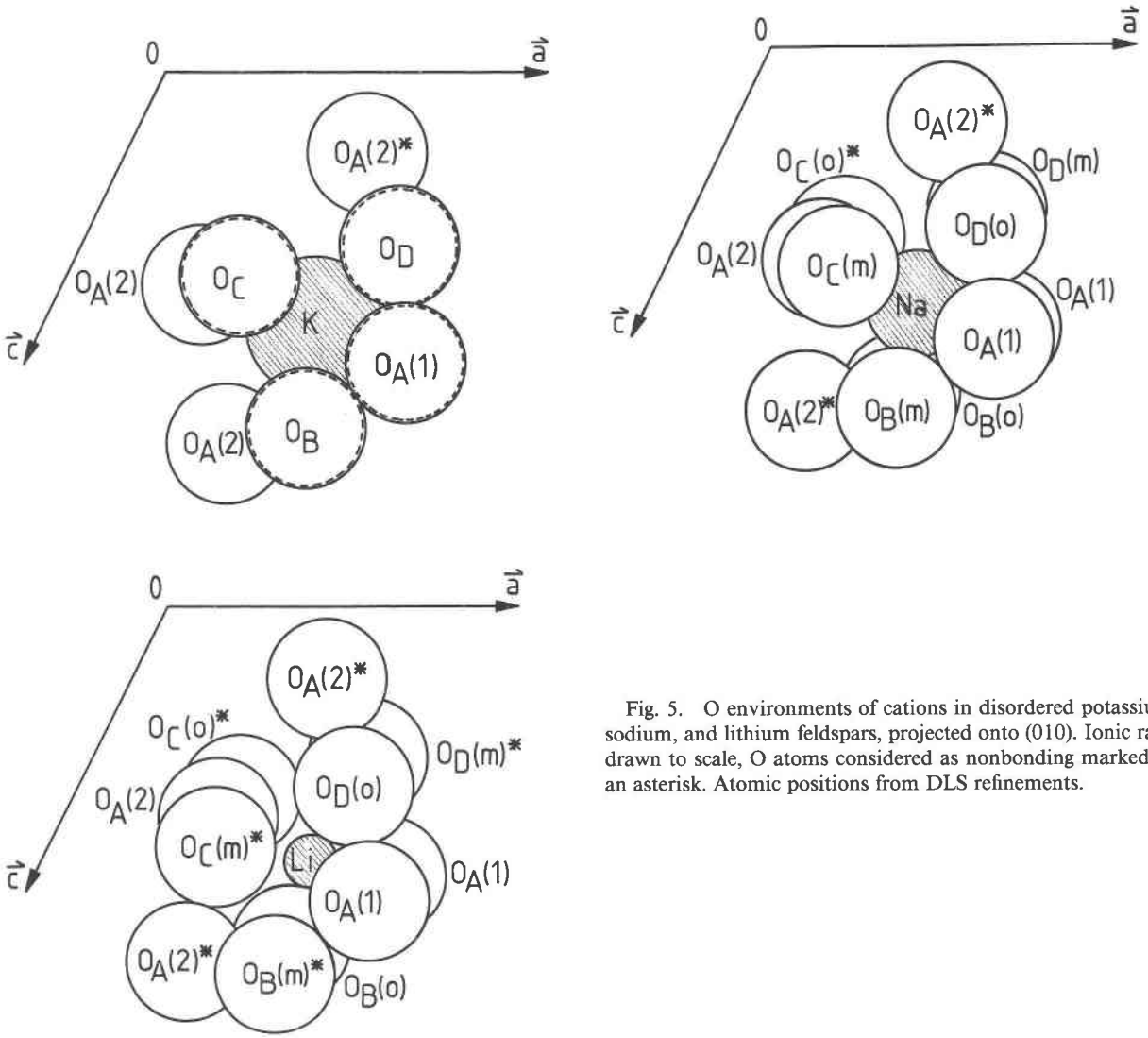

Fig. 5. O environments of cations in disordered potassium, sodium, and lithium feldspars, projected onto (010). Ionic radii drawn to scale, O atoms considered as nonbonding marked by an asterisk. Atomic positions from DLS refinements.

Conclusions

By low-temperature ion exchange, phases with feldspar structure and approximate composition $HAlSi_3O_8$, $LiAlSi_3O_8$, and $AgAlSi_3O_8$ can be prepared but only with essentially disordered Al-Si distribution in the framework. Lithium and silver feldspars are similar to sodium feldspar (analbite). They both obey the structural trends known from the natural alkali feldspars, whereas hydrogen feldspar does not.

Silver feldspar could be a stable phase: it is structurally intermediate between analbite and sanidine. However, Ag is more electronegative than the alkali metals and tends to form compounds with polarizable anions. Therefore, neither silver feldspars nor other silver silicates have been found in nature. The fact that hydrogen feldspar or other H-framework aluminosilicates are not stable is related to the particular stereochemistry of H. Whereas larger ions can distribute formal charge over all O atoms of their coordination polyhedra, protons can form bonds to only one or two anionic neighbors, which leads to heavy local overbonding.

With Li, the situation is different: lithium aluminosilicates such as β-eucryptite or β-spodumene are stable phases at elevated temperatures. These phases, however, have cation sites with four O neighbors at a distance around 2 Å that are well suited for Li ions. By contrast, the framework around the cation cavity in the feldspar structure is not flexible enough to provide a suitable Li coordination.

Acknowledgment

Support of this work by the Deutsche Forschungsgesellschaft is gratefully acknowledged.

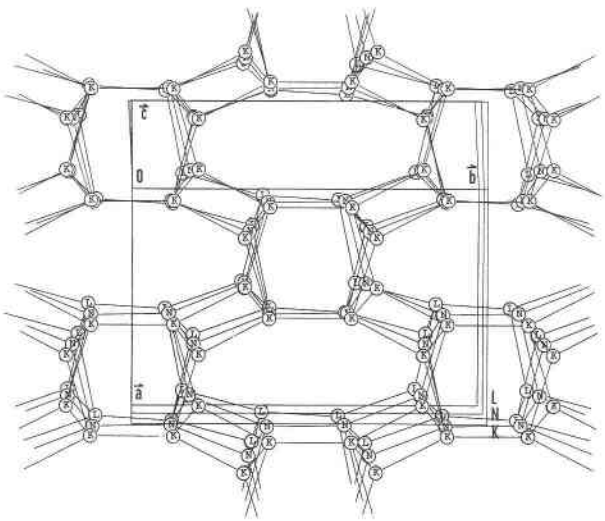

Fig. 6. Tetrahedral nodes of frameworks of disordered potassium, sodium, and lithium feldspars superimposed and projected onto (001). Positions of nodes from DLS refinements. K,N,L marks T positions in potassium, sodium, and lithium feldspars.

References cited

Baerlocher, C., Hepp, A., and Meier, W.M. (1978) DLS-76, a program for the simulation of crystal structures by geometric refinement. ETH, Zurich.

Beran, A. (1986) A model of water allocation in alkali-feldspars, derived from infrared-spectroscopic investigations. Physics and Chemistry of Minerals, 13, 306–310.

Bertelmann, D., Förtsch, E., and Wondratschek, H. (1985) Zum Temperverhalten von Sanidinen: Die Ausnahmerolle der Eifelsanidin-Megakristalle. Neues Jahrbuch für Mineralogie Abhandlungen, 152, 123–141.

Brown, I.D., and Altermatt, D. (1985) Bond-valence parameters obtained from a systematic analysis of the inorganic crystal structure database. Acta Crystallographica, B41, 244–247.

Effenberger, H., and Müller, G. (1988) Crystal structure and hydrogen bonding in H-petalite, $HAlSi_4O_{10}$. Zeitschrift für Kristallographie und Mineralogie, 185, 490.

Gasperin, M. (1971) Structure cristalline de $RbAlSi_3O_8$. Acta Crystallographica, B27, 854–855.

Gering, E. (1985) Silizium/Aluminium-Ordnung und Kristallperfektion von Sanidinen. Thesis, Kernforschungszentrum Karlsruhe, KfK 3984.

Henderson, C.M.B. (1979) An elevated temperature X-ray study of synthetic disordered Na-K alkali feldspars. Contributions to Mineralogy and Petrology, 70, 71–79.

Kroll, H. (1984) Thermal expansion of alkali feldspars. In W.L. Brown, Ed., Feldspars and feldspathoids. Structures, properties and occurrences, p. 163–205. Reidel, Boston.

Kroll, H., and Ribbe, P.H. (1983) Lattice parameters, composition and Al,Si order in alkali feldspars. In Mineralogical Society of America Reviews in Mineralogy, 2, 57–99.

Meier, W.M., and Villiger, H. (1969) Die Methode der Abstandsverfeinerung zur Bestimmung der Atomkoordinaten idealisierter Gerüststrukturen. Zeitschrift für Kristallographie und Mineralogie, 129, 411–423.

Müller, G. (1988) Preparation of hydrogen and lithium feldspars by ion exchange. Nature, 332, 435–436.

Müller, G., Hoffmann, M., and Neeff, R. (1988) Hydrogen substitution in lithium-aluminosilicates. Journal of Material Science, 23, 1779–1785.

Paulus, H., and Müller, G. (1988) The crystal structure of a hydrogen feldspar. Neues Jahrbuch für Mineralogie Monatshefte, H.11, 481–490.

Prewitt, C.T., Sueno, S., and Papike, J.J. (1976) The crystal structures of high albite and monalbite at high temperatures. American Mineralogist, 61, 1213–1225.

Shannon, R.D. (1976) Revised effective ionic radii and systematic studies of interatomic distances in halides and chalcogenides. Acta Crystallographica, A32, 751–767.

Smith, J.V., and Brown, W.L. (1988) Feldspar minerals, vol 1. Springer, Berlin.

Sternitzke, M., and Müller, G. (1991) Crystal structure and thermal expansion of quartz-type aluminosilicates. Journal of Material Science, 26, 3051–3056.

Vogt, T., Paulus, H., Fuess, H., and Müller, G. (1990) The crystal structure of $HAlSi_2O_6$ with a keatite-type framework. Zeitschrift für Kristallographie und Mineralogie, 190, 7–18.

Wright, T.L., and Stewart, D.B. (1968) X-ray and optical study of alkali feldspars. American Mineralogist, 35, 38–87.

Manuscript received November 5, 1990
Manuscript accepted May 14, 1991